

STRATLEARN-Z: IMPROVED PHOTO-Z ESTIMATION FROM SPECTROSCOPIC DATA SUBJECT TO SELECTION EFFECTS

CHIARA MORETTI^{1,2,3,4} , MAXIMILIAN AUTENRIETH⁵ , RICCARDO SERRA¹, ROBERTO TROTTA^{1,2,3,6}, DAVID A. VAN DYK⁵ , AND ANDREI MESINGER^{2,7}

¹SISSA - International School for Advanced Studies, Via Bonomea 265, 34136 Trieste, Italy

²Centro Nazionale “High Performance Computer, Big Data and Quantum Computing”

³INAF – Osservatorio Astronomico di Trieste, Via Tiepolo 11, I-34143 - Trieste, Italy

⁴INFN sezione di Trieste

⁵Statistic Section, Department of Mathematics, Imperial College London, 180 Queen’s Gate, London SW7 2AZ, UK

⁶Department of Physics, Imperial College London, Blackett Laboratory, Prince Consort Rd, SW7 2AZ London, UK and

⁷Scuola Normale Superiore (SNS), Piazza dei Cavalieri 7, Pisa, PI, 56125, Italy

Version October 1, 2024

ABSTRACT

A precise measurement of photometric redshifts (photo- z) is crucial for the success of modern photometric galaxy surveys. Machine learning (ML) methods show great promise in this context, but suffer from covariate shift in training sets due to selection bias where interesting sources, e.g., high redshift objects, are underrepresented, and the corresponding ML models exhibit poor generalisation properties. We present an application of the *StratLearn* method to the estimation of photo- z (*StratLearn-z*), validating against simulations where we enforce the presence of covariate shift to different degrees. *StratLearn* is a statistically principled approach which relies on splitting the combined source and target datasets into strata, based on estimated propensity scores. The latter is the probability for an object in the dataset to be in the source set, given its observed covariates. After stratification, two conditional density estimators are fit separately within each stratum, and then combined via a weighted average. We benchmark our results against the GPz algorithm, quantifying the performance of the two algorithms with a set of metrics. Our results show that the *StratLearn-z* metrics are only marginally affected by the presence of covariate shift, while GPz shows a significant degradation of performance, specifically concerning the photo- z prediction for fainter objects for which there is little training data. In particular, for the strongest covariate shift scenario considered, *StratLearn-z* yields a reduced fraction of catastrophic errors, a factor of 2 improvement for the RMSE as well as one order of magnitude improvement on the bias. We also assess the quality of the predicted conditional redshift estimates using the probability integral transform (PIT). The PIT distribution obtained from *StratLearn-z* features far fewer outliers and is symmetric, i.e., the predictions appear to be well-centered around the true redshift value, despite showing a rather conservative estimation of the spread of the conditional redshift distributions. Our JULIA implementation of the method, *StratLearn-z*, is publicly available at <https://github.com/chiamoretti/StratLearn-z>.

1. INTRODUCTION

The main science driver for current and planned cosmological experiments is the exploration of the dark sector. Stage-IV Dark Energy surveys, such as Euclid (Laureijs et al. 2011; Euclid Collaboration et al. 2024), the Vera C. Rubin Observatory Legacy Survey of Space and Time (LSST, The LSST Dark Energy Science Collaboration et al. (2018); Ivezić et al. (2019)), and Roman Space Telescope (Akeson et al. 2019), will pursue this goal by mapping the Universe over unprecedented volumes, delivering high precision measurements of cosmological observables. Of key importance for such measurements is our ability to produce accurate estimates of redshift for billions of sources.

The most precise way to estimate redshifts is via spectroscopic observations. These, however, are demanding in terms of observational time, and challenging for faint, high-redshift objects: the sheer number of sources in future surveys will prevent spectroscopic follow-up for the vast majority. A viable and well established alternative is provided by the so-called photometric redshift (photo- z , see e.g., Salvato et al. (2019); Brescia et al. (2021); Newman & Gruen (2022) for detailed

reviews), which are extracted from broadband flux measurements performed at different wavelengths. This approach, albeit far less accurate than spectroscopy, allows researchers to measure several objects simultaneously through imaging, as well as extending surveys to deeper regions.

Accuracy and precision in the estimation of photo- z are essential for the success of both current and future imaging surveys. In fact, systematic errors in the determination of redshifts from photometric observations can introduce biases into inferred cosmological parameters. Specifically, the lensing analysis relies on the construction of tomographic redshift bins, with minimal overlap between adjacent bins and a precise determination of the mean redshift of each bin (Ma et al. 2006; Amara & Réfrégier 2007). On the other hand, the clustering signal used in the 3x2pt analysis requires both the mean redshift and the width of the redshift distribution to be known with high accuracy (Tutusaus et al. 2020; Porredon et al. 2022). There are two main approaches for estimating photo- z : template-fitting methods and machine learning (ML) based methods. The former are based on matching the observed photometry to catalogs of template galaxy spectra in order to extract the galaxy redshifts; these methods rely on the completeness of such catalogs. Publicly available template-

fitting codes include LE_{PHARE} (Arnouts et al. 1999; Ilbert et al. 2006), BPZ (Benítez 2000), HYPERZ (Bolzonella et al. 2000) and EAZY (Brammer et al. 2008). On the other hand, the advent of ML techniques has opened new ways to improve photo- z estimation, taking advantage of artificial neural networks (Firth et al. 2003; Collister & Lahav 2004; Graff et al. 2014) random forests (Carliles et al. 2010; Carrasco Kind & Brunner 2013), self-organizing maps (Carrasco Kind & Brunner 2014; Masters et al. 2015), advanced ANNs (Sadeh et al. 2016), Gaussian processes (Almosallam et al. 2016a,b), nearest neighbors (Graham et al. 2018), convolutional neural networks (Pasquet et al. 2019; Henghes et al. 2022) and graph neural networks (Tosone et al. 2023).

Indeed, ML methods have successfully been applied to Stage-III surveys: both the Dark Energy Survey (DES, Abbott et al. (2018)) and the Kilo-Degree Survey (KiDS, Heymans et al. (2021)) have used self-organizing maps to estimate photo- z (see Myles et al. (2021) and Hildebrandt et al. (2021) respectively), while the Hyper Suprime-Cam (HSC, Aihara et al. (2018)) adopted conditional density estimators (Rau et al. 2023; Sugiyama et al. 2023). Performance analyses comparing different approaches have also been presented (Hildebrandt et al. 2010; Sánchez et al. 2014). In preparation for Stage-IV surveys, several ML methods have been compared with each other and to template-fitting methods, in particular for Euclid (Euclid Collaboration et al. 2020) and for LSST-DESC (Schmidt et al. 2020).

ML methods rely on source datasets used to train the algorithms where both spectroscopic and photometric observations are available, in order to learn the relationship between the observed photometry and redshift. A significant issue is posed by non-representative training sets, i.e., spectroscopic training samples that are not random samples from the target photometric survey. Indeed, such non-representative samples are the usual situation in astronomy, where the lack of representativeness is a generic and widespread consequence to selection bias. An example is ‘Malmquist bias’, (Malmquist 1922, 1925)), which results in spectroscopic catalogs being biased towards brighter, lower redshift sources. Observational biases can thus result in different distributions for the covariates of the source datasets, used to train the ML algorithms, and the target dataset, for which we wish to estimate photo- z . Under the assumption that the conditional distribution of the outcome (in this context, the redshift) given the covariates (colors/magnitudes) is the same in the source and target group, the effect is known as covariate shift (Moreno-Torres et al. 2012) in the ML literature. The impact of covariate shift on photo- z estimation has been investigated in Freeman et al. (2017), where the authors propose to mitigate the effect of covariate shift with the use of importance weights, and apply the proposed method to data from DR8 of the Sloan Digital Sky Survey. More recently, Stylianou et al. (2022) investigates the performance of GPz (Almosallam et al. 2016a,b), an algorithm based on Gaussian processes, applying it to simulations that feature imperfections in the spectroscopic training set. Additionally, Toribio San Cipriano et al. (2023) studies the impact of incompleteness of the training set in the context of DES, while Moskowitz et al. (2024) suggests a method to augment the training sample to improve photo- z estimation.

In this work, we focus on *StratLearn* (Autenrieth et al. 2024b; Autenrieth et al. 2024a), a statistically motivated approach that improves the performance of ML-based algorithms in the presence of covariate shift. *StratLearn* splits the data into subgroups, or strata, based on the estimated propensity scores,

which in the context of this paper is the probability of a galaxy in the data set being included in the spectroscopic source set, given its observed covariates (magnitudes or colors). Propensity scores are balancing scores, and a pivotal methodology in causal inference (Rosenbaum & Rubin 1983). Conditioning on the propensity scores via stratification approximately balances within strata the covariates of source and target data, which then improves the fitting of ML methods within each stratum (Autenrieth et al. 2024b). In this paper we apply an implementation of the *StratLearn* method, *StratLearn-z*, to photo- z estimation, and assess its performance on simulated data with different degrees of covariate shift, with a view to future surveys such as Euclid and LSST. Our goal is to showcase the ability of *StratLearn-z* to provide accurate photo- z estimates even in presence of strong covariate shift, which can reduce systematic biases and therefore be highly beneficial for such experiments.

The paper is organized into four additional sections: in Sec. 2 we present the problem of covariate shift and review *StratLearn*. In Sec. 3 we describe the dataset and the procedure we adopt to introduce covariate shift in the dataset. In Sec. 4 we present our results and comment on them in Sec. 5. Throughout, we refer to the implementation of *StratLearn* adopted here as *StratLearn-z*.

2. STRATLEARN – ADDRESSING COVARIATE SHIFT

In this section we present in more detail the covariate shift problem in the context of photo- z estimation, and summarize the *StratLearn* approach developed in Autenrieth et al. (2024b).

2.1. Covariate shift in non-representative spectroscopic data

Starting from a source dataset of labelled observations with spectroscopic redshift $z^{(i)}$ and covariates $x^{(i)}$ (photometric magnitudes or colors), we aim to obtain redshift estimations for a much larger target set of unlabelled sources, i.e., for sources with only photometric information/covariates available. The source dataset $D_S = \{(x_S^{(i)}, z_S^{(i)})\}_{i=1}^{N_S}$ consists of N_S galaxies sampled from the joint distribution $p_S(x, z)$, while the target dataset $D_T = \{x_T^{(i)}\}_{i=1}^{N_T}$ consists of N_T galaxies sampled from the joint distribution $p_T(x, z)$, with $N_T \gg N_S$. Selection effects induce differences between the source and target distributions, $p_S(x) \neq p_T(x)$, leading to $p_S(x, z) \neq p_T(x, z)$. However, we assume that the conditional distribution of redshifts given the covariates is the same for both source and target, $p_S(z|x) = p_T(z|x)$. This situation is known to affect the performances of ML algorithms, because the patterns learned from the (unrepresentative) source set do not generalise properly to the target set. ¹

2.2. *StratLearn*

StratLearn is designed to improve the generalisation properties of ML algorithms in presence of covariate shift. While the method is general and applicable to both classification and regression problems, we focus here on photo- z estimation, as discussed in the previous section. In the following we denote all estimated quantities with a hat symbol, e.g., \hat{p} .

¹ We note that the assumption $p_S(z|x) = p_T(z|x)$ may not always hold, e.g. in case of additional selection bias in the identification of a reliable spectroscopic redshift (Hartley et al. 2020) (see also the discussion in Sec. 5). We plan to explore such cases in a future work.

The approach relies on stratification of data into sub-groups, or strata, based on propensity scores, i.e., the estimated probability for an object i in the dataset to be in the source set ($s_i = 1$) given the observed covariates x_i :

$$e(x_i) = P(s_i = 1 | x_i), \quad (1)$$

with the assumption that $0 < e(x_i) < 1$. For each object we obtain an estimate of the propensity score $\hat{e}(x_i)$ via binary classification of source and target data. Specifically, we employ a logistic regression model with all photometric magnitudes/colors as covariates, and group the data in K strata based on the quantiles of the estimated propensity score distribution. We use $K = 5$ strata, as it has been shown that this number is able to remove at least 90% of the bias for many distributions (Cochran 1968; Rosenbaum & Rubin 1983). The stratification process balances the covariate distribution in the source and target sets (Rosenbaum & Rubin 1983), resulting in $p_{T_j}(z, x) \simeq p_{S_j}(z, x)$, for $j = 1, \dots, K$, where the subscript T_j denotes conditioning on assignment to the j -th target stratum (and analogously, S_j for source stratum).

We use a weighted average of two supervised full conditional density estimators, trained separately in each stratum, to obtain a non-parametric estimate of the full galaxy photo- z conditional densities of each object in the target set, $\hat{p}_T(z | x)$, conditional on its observed covariates. We adopt the *ker-NN* estimator proposed in Freeman et al. (2017) and the *Series* estimator described in Izbicki et al. (2016): the former relies on a kernel smoothed histogram of the redshift of the k nearest neighbors to x , within each stratum, to compute the conditional redshift distribution, while the latter adapts a lower-dimensional subspace of the covariates, x , as the intrinsic dimension of the data, based on data-dependent eigenfunctions of a kernel based estimator. Our choice of conditional density estimators is based on good performance shown in previous work, e.g., Autenrieth et al. (2024b). However, generally, the *StratLearn* framework could be combined with any model.

We fit the two models using the labelled spectroscopic source data as a training set, and obtain an estimate of the redshift distribution for each galaxy in the photometric target data. If the source set is representative of the target set, conditional density estimators commonly aim to minimize the generalized risk under the L^2 -loss:

$$\hat{R}_S(\hat{p}) = \frac{1}{N_S} \sum_{k=1}^{N_S} \int \hat{p}^2(z | x_S^{(k)}) dz - 2 \frac{1}{N_S} \sum_{k=1}^{N_S} \hat{p}(z_S^{(k)} | x_S^{(k)}), \quad (2)$$

where the subscript ‘ S ’ indicates the source set, $z_S^{(k)}$ is the redshift and $x_S^{(k)}$ refers to the covariates for the k -th object in the source set. We notice however that the presence of covariate shift requires minimisation of the *target* risk $\hat{R}_T(\hat{p})$ in order to obtain accurate target estimates, which in turn would require having access to the target redshifts. The stratification procedure described above allows for minimisation of $\hat{R}_{T_j}(\hat{p})$ via minimisation of $\hat{R}_{S_j}(\hat{p})$ within each stratum j (see Autenrieth et al. (2024a) for a more detailed description). Finally, the two conditional density estimators are combined via

$$\hat{p}(z | x) = (1 - \alpha) \hat{p}_{\text{Series}}(z | x) + \alpha \hat{p}_{\text{ker-NN}}(z | x), \quad (3)$$

where $0 \leq \alpha \leq 1$ is a weight parameter. This requires a further optimisation to compute α (within each stratum) via

minimisation of the generalised risk:

$$\hat{R}_{S2_j}(\hat{p}) = \frac{1}{N_{T_j}} \sum_{k=1}^{N_{T_j}} \int \hat{p}^2(z | x_T^{(k)}) dz - 2 \frac{1}{N_{S_j}} \sum_{k=1}^{N_{S_j}} \hat{p}(z_S^{(k)} | x_S^{(k)}). \quad (4)$$

3. SIMULATED DATASET

To assess the performance of *StratLearn* we make use of a simulated dataset derived from the Buzzard Flock² simulation suite (DeRose et al. 2019), initially developed for DES. In particular, we adopt the LSST-DESC DC1 mock catalog used in Stylianou et al. (2022)³, consisting of a sample of 100,000 galaxies with redshift range $0 < z < 2.3$ and complete photometry in the *ugrizy* bands, from which we compute colors to serve as input covariates to our algorithm.

The dataset was constructed from the catalogs described in Schmidt et al. (2020) (specifically, see Sec. 2 of that work and the references therein for a more detailed description of the dataset). Stylianou et al. (2022) uses this dataset to study the impact of systematics in the training dataset on the the GPz algorithm (Almosallam et al. 2016a,b). Particular attention is paid to two possible degradations in the training dataset that might affect the performance of the algorithm: redshift incompleteness and emission line confusion. The redshift incompleteness in particular is similar to what we explore here, we therefore use GPz to benchmark the performance of *StratLearn-z*. However, we introduce incompleteness (and therefore, lack of representativeness) in the training data via a different prescription, as detailed in Sec. 3.1.

3.1. Introducing covariate shift

We enforce covariate shift in the dataset by performing rejection sampling on the the r -band, to obtain the target data, following Izbicki et al. (2016). This approach is designed to mimic a selection effect that biases the source set towards brighter objects, similar to what happens with real observations. Specifically, we resample the full dataset via rejection sampling, assigning each galaxy to the target set with probability $p(s = 0 | x) = f_{B(\alpha, \beta)}(x_r) / \max_{x_r} f_{B(\alpha, \beta)}(x_r)$, where $f_{B(\alpha, \beta)}$ is the density of a beta random variable with parameters α, β and the r -band magnitudes, x_r , are re-scaled to be between 0 and 1. Galaxies not assigned to the target set are assigned to the source data.

We consider four different scenarios with different degrees of covariate shift (CS):

- no CS: data are randomly split between source and target sets;
- weak CS: $\alpha = 4, \beta = 5$;
- mild CS: $\alpha = 5, \beta = 6$;
- strong CS: $\alpha = 5, \beta = 7$.

From this procedure we obtain four source datasets, three of which have r -band distributions that are shifted with respect to their corresponding target datasets, as shown in Fig. 1 for the various covariate shift cases. Although in a simplified form, the rejection sampling procedure mimics the effect of selection

² <https://buzzardflock.github.io/index.html>

³ Specifically, the catalogue distributed with the pzflow package (Crenshaw et al. 2024) at https://github.com/jfcrenshaw/pzflow/blob/main/pzflow/example_files/galaxy-data.pkl

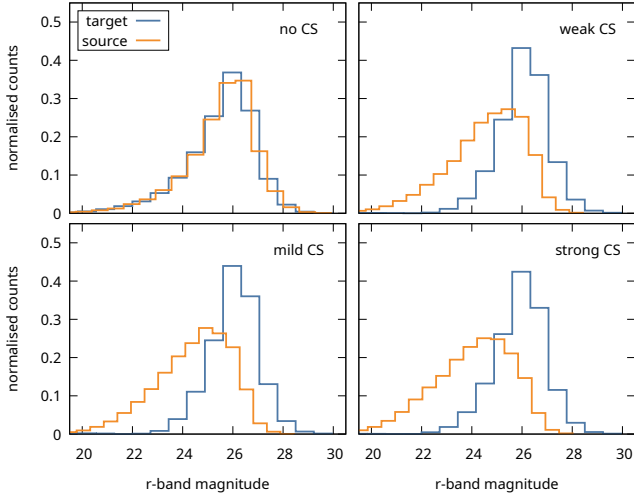


FIG. 1.— Source and target normalised distributions of r -band magnitudes for the four covariate shift cases, as stated in each panel. Orange histograms represent the source (labelled) datasets, while in blue we plot the target (unlabelled) datasets. Notice how the rejection sampling procedure introduces a shift – to different degrees, based on the chosen parameters (i.e. scenarios) – between the source and target sets.

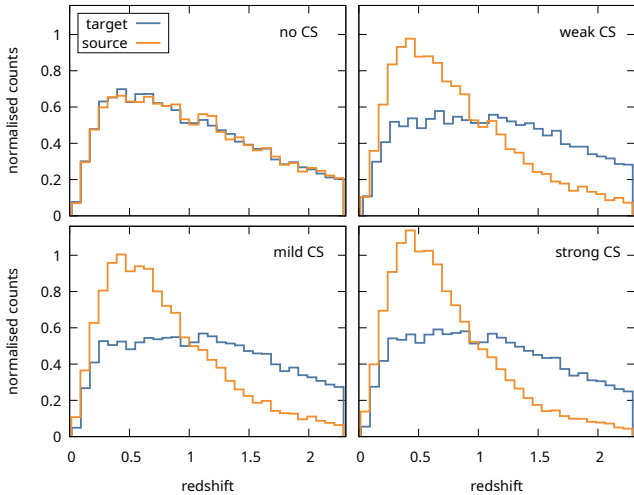


FIG. 2.— Source and target normalised redshift distributions for the four covariate shift cases, as obtained after the rejection-sampling procedure described in Sec. 3.1. Orange histograms represent the source datasets, while in blue we plot the target datasets. We plot the true redshift distribution for the target data, which in reality is of course unknown.

bias in real data, where the limiting magnitude of the r -band distribution of spectroscopic observations is usually at lower values than for photometric observations (see e.g., Fig. 3 of Izbicki et al. 2016), because of higher probability of detecting brighter objects. Such bias is also visible as a shift in the redshift distributions for source and target, as shown in Fig. 2: the source set features a peak at lower redshifts, that is more pronounced the stronger the covariate shift. We also plot the distributions for all other photometric bands in Appendix A.

The rejection sampling procedure described above results in source and target datasets of very different sizes among the four CS scenarios. To focus on the impact of covariate shift, and remove dependence of the results on the size of the datasets, we want the source sets for all scenarios to have the same size (and similarly for the target sets). Thus, we randomly

resample the sets to construct the source datasets, used to train the conditional density estimators, and target datasets, used to compute performance metrics.

Specifically, we randomly sub-sample 20,000 objects for each training set and 63,000 in each target set, except the target dataset in the weak CS scenario was not sub-sampled because rejection sampling yielded only 62,000 objects.

We choose the target sets to be significantly larger than the training sets to reproduce what happens with real data, where labels (spectroscopic redshifts) are only available for a small fraction of the total photometric measurements. For example, Euclid is expected to observe photometry for ~ 1.5 billion galaxies, of which only ~ 25 million will have redshift measurements obtained from slitless spectroscopy (Euclid Collaboration et al. 2024).

3.2. StratLearn computation

For each scenario, we estimate the propensity scores using a logistic regression model to predict the binary classification into the source and target data. In particular, we use the r -band data and colors obtained from all other available photometric bands as covariates (i.e., $u - g$, $g - r$, $r - i$, $i - z$, $z - y$). We then partition each of the datasets (combining source and target data under each scenario) into five strata, based on the quintiles of the corresponding propensity score distributions. The resulting strata are populated as detailed in Table 1. The no CS case results in approximately equally sized strata: ~ 4000 in the source set and ~ 12500 in the target set, per stratum. For the datasets with covariate shift there is significantly more data in the first source strata (corresponding to a lower mean redshift), as expected.

Fig. 3 plots the distributions of the r -band magnitudes for the source and target sets within each stratum of the strong CS scenario. Stratification achieves approximately balanced distributions within each strata. Additionally, stratification results in a redshift partition, where in each stratum the mean redshift of the source data approximately matches the mean redshift of the target data – an indication that stratification is approximately removing covariate shift (Autenrieth et al. 2024b) within each stratum. Redshift distribution for source and target sets for the strong CS case are shown in Fig. 15 of Appendix B, showcasing once again the effectiveness of StratLearn to improve balance within each stratum.

We train the ker-NN and Series conditional density estimators separately within each stratum, and combine them using Eq. 3 to obtain an estimate of the conditional distribution of redshift for each object in the target set. We emphasize that only the source redshifts are used to train the models, while the target redshifts are used exclusively to evaluate performance metrics. The estimated (photometric) redshift \hat{z}_{photo} , computed as the mean of the estimated conditional redshift distribution, is compared to the true (spectroscopic) redshift z_{spec} for each galaxy in the target dataset, and performance in each covariate shift scenario is assessed using several metrics (see Sec. 4). As discussed in Sec. 3, we benchmark our results against the GPz code run on the same datasets.

4. StratLearn- z PERFORMANCE

We evaluate the performance of StratLearn- z in terms of both its point estimate \hat{z}_{photo} and its estimate of the conditional distribution of redshift via several metrics applied to the conditional densities obtained for the target dataset.

To obtain more robust numerical results for the performance metrics we run 15 different realisations for each covariate shift

TABLE 1

Balance between strata after propensity score estimation, for the four covariate shift scenarios. We also report the mean redshift of each stratum for both the source and target datasets. A similar value for the mean redshift within strata indicates that the source and target data are balanced, although we note that this diagnostic is not possible in practice with real source/target data, as z is not observed in the target dataset.

Stratum	No CS		weak CS		mild CS		strong CS	
	Size	Mean z	Size	Mean z	Size	Mean z	Size	Mean z
1 (source)	4113	1.298	9959	0.625	10470	0.617	11038	0.571
1 (target)	12487	1.306	6441	0.708	6130	0.705	5562	0.666
2 (source)	4053	1.313	4479	0.899	4643	0.894	4764	0.850
2 (target)	12547	1.311	11921	0.904	11957	0.887	11836	0.854
3 (source)	3978	1.051	2799	0.979	2644	0.954	2432	0.963
3 (target)	12622	1.058	13601	0.984	13956	0.972	14168	0.962
4 (source)	3929	0.740	1917	1.113	1549	1.130	1253	1.061
4 (target)	12671	0.753	14483	1.121	15051	1.108	15347	1.075
5 (source)	3927	0.644	846	1.498	694	1.469	513	1.406
5 (target)	12673	0.624	15554	1.579	15906	1.585	16087	1.525
total (source)	20000	1.014	20000	0.820	20000	0.795	20000	0.737
total (target)	63000	1.009	62000	1.121	63000	1.117	63000	1.087

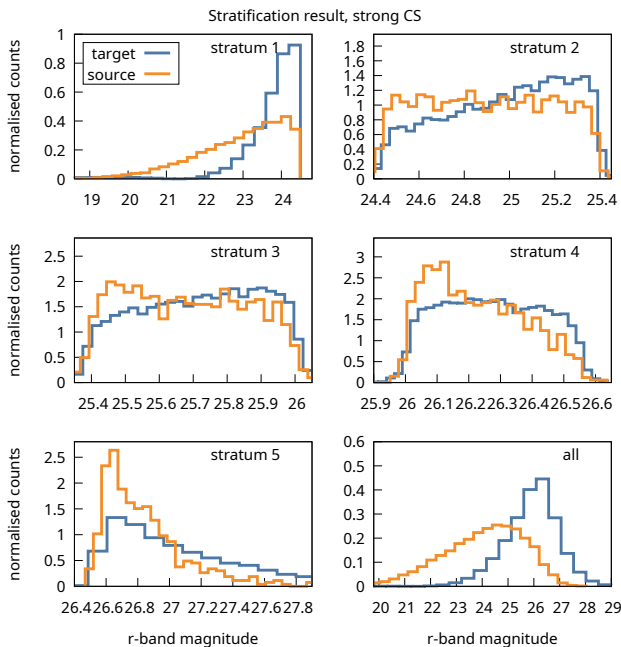


FIG. 3.— Distribution of r-band magnitudes for source (orange histograms) and target (blue histograms) sets for the strong CS scenario, after performing stratification based on estimated propensity scores. In the lower right panel, where we plot the full source and target sets, the distributions are significantly different, while in the other panels, representing each a different stratum, we are able to achieve improved balance.

scenario. The datasets for each realisation are obtained as follows:

- the full dataset is randomly permuted;
- rejection sampling as described in Sec. 3.1 is applied to the randomly permuted dataset, once per covariate shift scenario, resulting in four different source/target sets;
- random sampling is applied to each set, so that source

sets have 20,000 objects and target sets have 63,000 objects (62,000 for the weak CS scenario, see Sec. 3.1).

The procedure is repeated 15 times, in order to obtain a total of 60 source/target sets, 15 for each covariate shift scenario. The models are trained separately on each source set, and conditional density estimations constructed for the respective target set. For each realisation, several performance metrics are then computed as described in the next section.

4.1. Point estimate metrics

The quality of the photo- z point estimate \hat{z}_{photo} is assessed by comparing it to the true redshift z_{spec} . Because we are working with simulated data, z_{spec} is available for all objects in the target set, which can therefore be used to compute performance metrics. We focus on the root mean square error (RMSE), the bias, and the fraction retained (FR). The latter provides an estimate of (100 times) the fraction of objects for which \hat{z}_{photo} does not exhibit catastrophic errors, defined as those objects for which residual differences between \hat{z}_{photo} and z_{spec} are above some large threshold, defined relative to specific survey requirements. FR corresponds therefore to the fraction of redshift estimates that are not catastrophic, i.e., are ‘good’ (see Eq.s 7 and 8 for the thresholds adopted here). The metrics are evaluated as follows:

- Root mean square error (RMSE):

$$\sqrt{\frac{1}{N_T} \sum_{i=1}^{N_T} (z_{\text{spec}}^{(i)} - \hat{z}_{\text{photo}}^{(i)})^2}; \quad (5)$$

- mean error, commonly referred to in the literature as ‘bias’:

$$\frac{1}{N_T} \sum_{i=1}^{N_T} (z_{\text{spec}}^{(i)} - \hat{z}_{\text{photo}}^{(i)}); \quad (6)$$

- FR15:

$$\frac{100}{N_T} \sum_{i=1}^{N_T} \left[\left| \frac{z_{\text{spec}}^{(i)} - \hat{z}_{\text{photo}}^{(i)}}{1 + z_{\text{spec}}^{(i)}} \right| < 0.15 \right]; \text{ and} \quad (7)$$

- FR05:

$$\frac{100}{N_T} \sum_{i=1}^{N_T} \left[\left| \frac{z_{\text{spec}}^{(i)} - \hat{z}_{\text{photo}}^{(i)}}{1 + z_{\text{spec}}^{(i)}} \right| < 0.05 \right]. \quad (8)$$

The RMSE and mean error used in the context of photo- z estimation are sometimes normalised by a factor $1 + z_{\text{spec}}$: this serves to down-weight the deviation from the spectroscopic redshift for high-redshift sources. For example, [Almosallam et al. \(2016a\)](#) and [Euclid Collaboration et al. \(2020\)](#) use the normalised definitions, while [Hartley et al. \(2020\)](#) and [Toribio San Cipriano et al. \(2023\)](#) use the un-normalised ones. We note that the choice of performance metrics in the literature is far from homogeneous. Given our benchmark against GPz, we adopt the metrics used in [Stylianou et al. \(2022\)](#), but report our results in terms of both the normalised and un-normalised metrics.

4.2. Conditional redshift distribution metrics

Measuring the precision of the conditional redshift distribution is more complicated, because there are no ‘true’ conditional redshift distributions available. One possibility is using the distribution of the probability integral transform (PIT, [Dawid \(1984\)](#), see also [Polsterer et al. \(2016\)](#)), defined as

$$\text{PIT} = \int_0^{z_{\text{spec}}} \hat{p}_T(z|x) dz, \quad (9)$$

where $\hat{p}_T(z|x)$ is the conditional redshift distribution prediction for the target set given the observed photometry x . Under the assumption that $\hat{p}_T(z|x)$ exactly represents the conditional distribution of the true redshift, z_{spec} , given x , PIT is uniformly distributed over the unit interval. On the other hand, shifts from uniformity in the PIT distribution suggest systematic deviations in the estimates of the conditional distributions of redshift, while over-estimation (under-estimation) of the spread of the conditional distribution of redshift, i.e., the uncertainty associated with the estimated \hat{z}_{photo} , appear as a bump (dip) in the histogram of PIT. The PIT distribution is commonly used to visually evaluate the quality of estimated photo- z distributions (see e.g. [Bordoloi et al. 2010](#); [Polsterer et al. 2016](#); [D’Isanto & Polsterer 2018](#); [Tanaka et al. 2018](#); [Euclid Collaboration et al. 2020](#)).

However, we note that the PIT distribution is not an indicator of the information content of the estimated conditional density. Indeed, [Schmidt et al. \(2020\)](#) shows that a method with no predictive power can produce a perfectly uniform PIT distribution. (See discussion of the TRAINZ estimator, which assigns the marginal redshift distribution of the source data to each galaxy in the target set. This distribution does not depend on the photometric data and produces the same photo- z estimate for every galaxy in the target set.)

4.3. Results and comparison to GPz

We compare the performance of *StratLearn-z* to the output of GPz ([Almosallam et al. 2016a,b](#)) for each of the four covariate shift scenarios, by running both codes on the

same datasets⁴. GPz is based on sparse Gaussian processes and produces input-dependent (in this context, photometry-dependent) variance estimates which take into account both the density of the source data and noise in the photometric observations. One drawback of GPz is that the predicted conditional redshift distribution is forced to be a unimodal Gaussian. The GPz code was compared to other existing photo- z software in [Schmidt et al. \(2020\)](#) for LSST and in the photometric challenge paper for Euclid ([Euclid Collaboration et al. 2020](#)); as is the case for other ML approaches, its performance is strongly dependent on the quality of the spectroscopic set used for training.

The 2D histograms in Fig. 4, 5, 6, and 7 show the true z_{spec} versus the estimated \hat{z}_{photo} , obtained as the mean of the predicted conditional redshift distribution, for each covariate shift scenario and for both *StratLearn-z* (left panels) and GPz (right panels). Visual inspection of the 2D histograms indicates that the GPz predictions are strongly degraded for high-redshift objects in the presence of covariate shift, where the distribution of $z_{\text{spec}} - \hat{z}_{\text{photo}}$ exhibits high variance. On the other hand, the *StratLearn-z* predictions are only marginally impacted by covariate shift, even in the worst case scenario shown in Fig. 7. We note that the plots refer to one specific realisation out of the 15 runs we perform for each case, however, a similar pattern is apparent for the remaining realisations.

We perform a more quantitative comparison of the redshift point-estimates by means of the performance metrics described in Sec. 4.1. The metrics are computed separately for each of the 15 resampled datasets and then averaged. Numerical results for the average performance metrics and standard deviations are collected in Table 2 and illustrated in Fig. 4.3.

We note that *StratLearn-z* outperforms GPz for all metrics and in all cases considered, even in the no CS case, which can likely be ascribed to better performance of the conditional density estimators. However, the difference is more pronounced with more covariate shift. Both the averaged RMSE and the normalised averaged RMSE, shown in the top panels of Fig. 4.3, show a similar trend: while for GPz they are nearly doubled when going from the case with no CS to the case with strong CS, they are only marginally impacted by the presence of covariate shift in the *StratLearn-z* results. Turning to the mean error, or bias (central left panel of Fig. 4.3), the impact of covariate shift on *StratLearn-z* leads to a mean error that is four times larger in the strong CS scenario with respect to the no CS case, while for GPz the increase is almost one order of magnitude. Moreover, we note that the averaged normalised error for *StratLearn-z* is always consistent with zero, except for the no CS case where it is slightly lower. Concerning the FR metric we find again that with *StratLearn-z* FR is consistent across covariate shift scenarios, with the FR15 (FR05) being only 0.5% (2.5%) worse in the strong CS case with respect to the no CS case. For GPz on the other hand FR15 decreases from ~ 99 in the no CS case to ~ 96 in the strong CS case. Similarly, the FR05 ranges from ~ 98 to ~ 95 for *StratLearn-z*, and from ~ 95.5 to ~ 85 for GPz.

To evaluate the predicted conditional redshift distributions, Fig. 9 plots the histogram of PIT obtained from *StratLearn-z* and GPz for the four scenarios, focusing on one specific realisation. We checked that the PIT histograms are not significantly different across the 15 realisations. We see a significant accu-

⁴ We use the GPz version distributed with [Stylianou et al. \(2022\)](#) and available from [https://github.com/nataliastylianou/photo-\\$z/tree/main](https://github.com/nataliastylianou/photo-$z/tree/main).

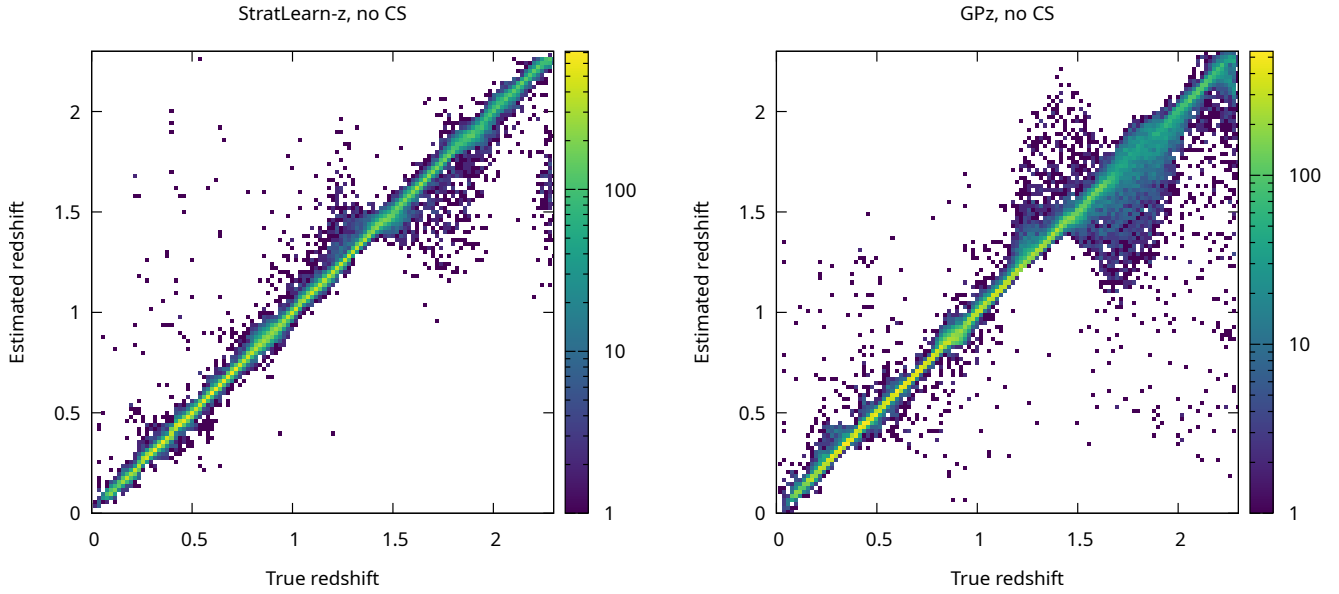


FIG. 4.— 2D histograms for the estimated \hat{z}_{photo} versus the true z_{spec} for the no CS case, $\alpha = 1$, $\beta = 1$. Left: *StratLearn-z*, right: GPz. The colorbar indicates the number of sources in each 2D bin.

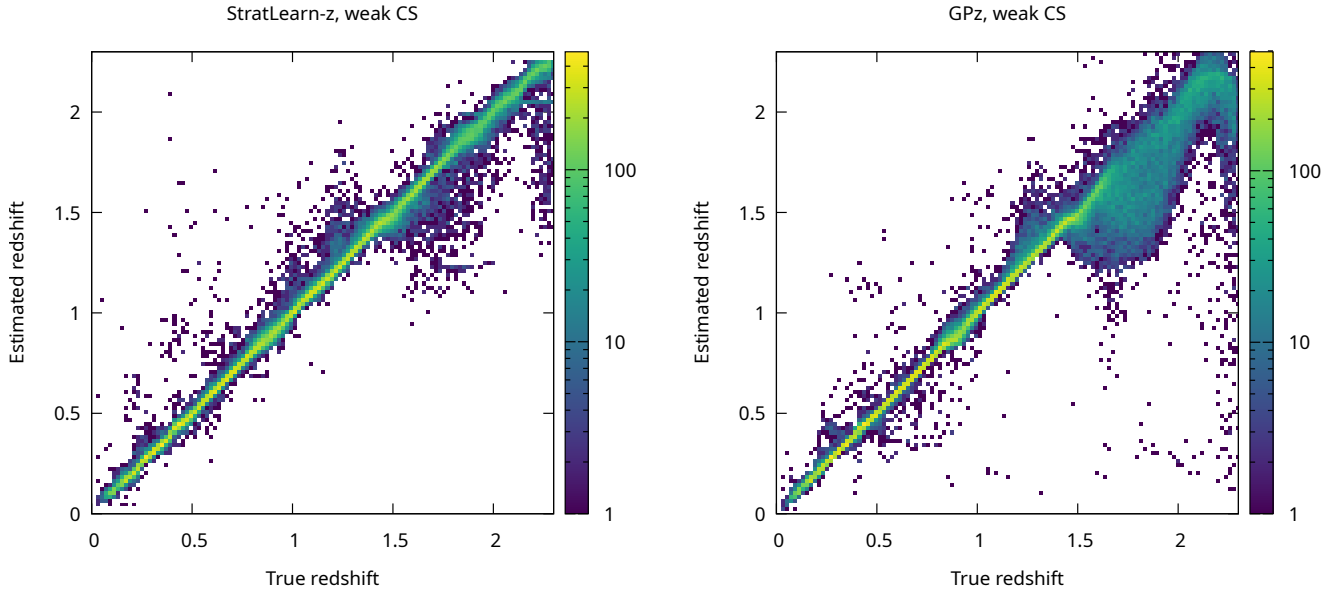


FIG. 5.— Same as Fig. 4, but for the weak CS case, $\alpha = 4$, $\beta = 5$. Left: *StratLearn-z*, right: GPz.

TABLE 2

Average performance metrics and the corresponding standard deviations for *StratLearn-z* and GPz for the four covariate shift scenarios considered.

	no CS		weak CS		mild CS		strong CS	
	<i>StratLearn-z</i>	GPz	<i>StratLearn-z</i>	GPz	<i>StratLearn-z</i>	GPz	<i>StratLearn-z</i>	GPz
RMSE	0.0583 ± 0.0036	0.0842 ± 0.0079	0.0697 ± 0.0073	0.1159 ± 0.0149	0.0724 ± 0.0054	0.1332 ± 0.0249	0.0817 ± 0.0010	0.1526 ± 0.0299
Norm. RMSE	0.0302 ± 0.0025	0.0363 ± 0.0020	0.0313 ± 0.0019	0.0431 ± 0.0032	0.0323 ± 0.0019	0.0483 ± 0.0071	0.0373 ± 0.0052	0.0547 ± 0.0086
Bias	0.0012 ± 0.0008	0.0043 ± 0.0027	0.0033 ± 0.0017	0.0218 ± 0.0080	0.0038 ± 0.0017	0.0292 ± 0.0114	0.0048 ± 0.0030	0.0376 ± 0.0155
Norm. bias	-0.0005 ± 0.0003	0.0005 ± 0.0010	0.0001 ± 0.0005	0.0068 ± 0.0029	0.0002 ± 0.0006	0.0094 ± 0.0039	0.0003 ± 0.0009	0.0122 ± 0.0053
FR15	99.46 ± 0.08	98.96 ± 0.15	99.24 ± 0.15	98.31 ± 0.44	99.19 ± 0.12	97.43 ± 0.97	98.99 ± 0.24	96.27 ± 1.53
FR05	97.81 ± 0.27	94.48 ± 0.78	96.59 ± 0.65	88.73 ± 2.30	96.14 ± 0.66	86.59 ± 3.29	95.25 ± 1.35	84.99 ± 3.33

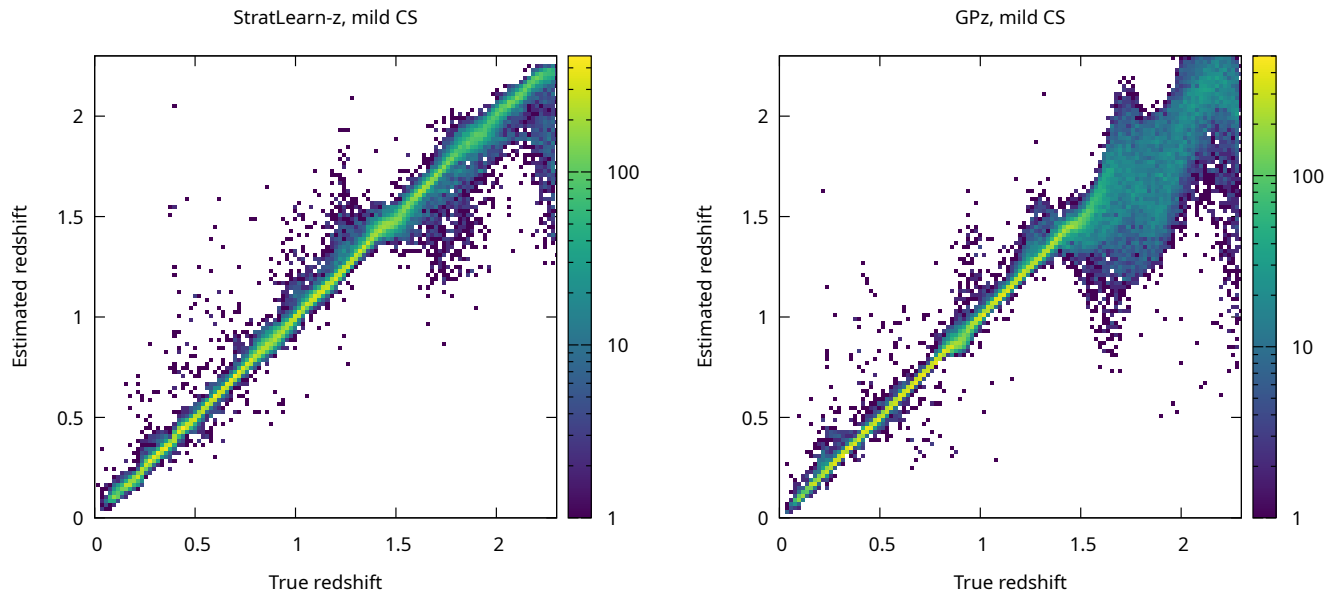


FIG. 6.— Same as Fig. 4, but for the mild CS case, $\alpha = 5$, $\beta = 6$. Left: *StratLearn-z*, right: *GPz*.

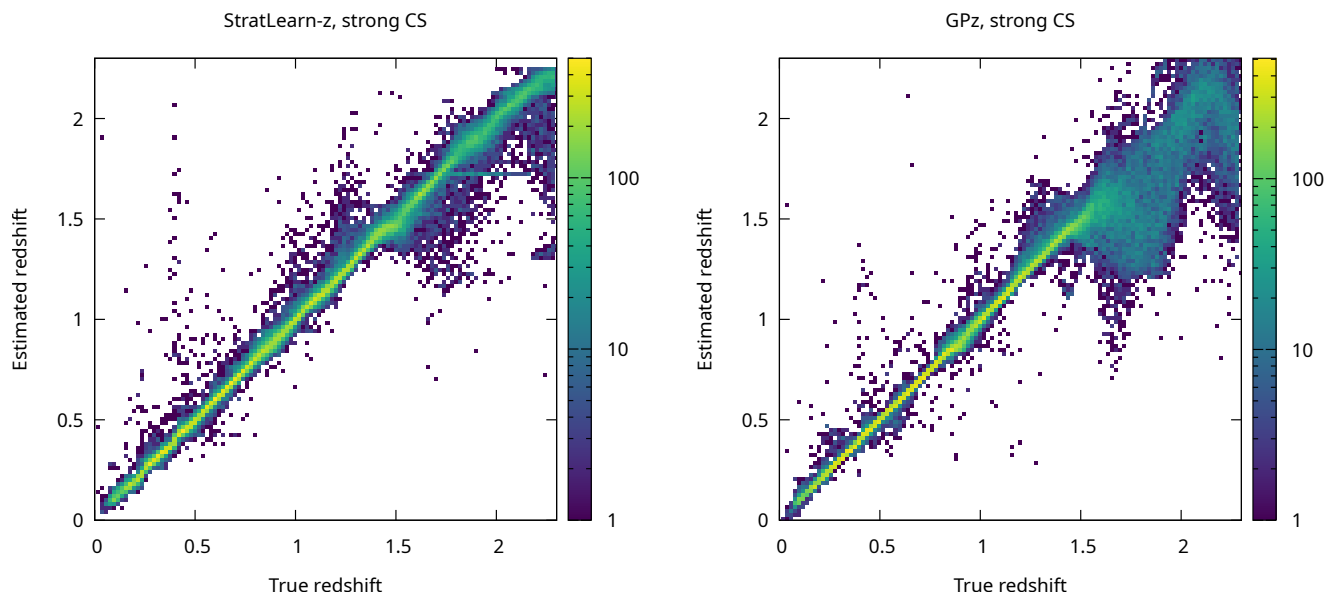


FIG. 7.— Same as Fig. 4, but for the strong CS case, $\alpha = 5$, $\beta = 7$. Left: *StratLearn-z*, right: *GPz*.

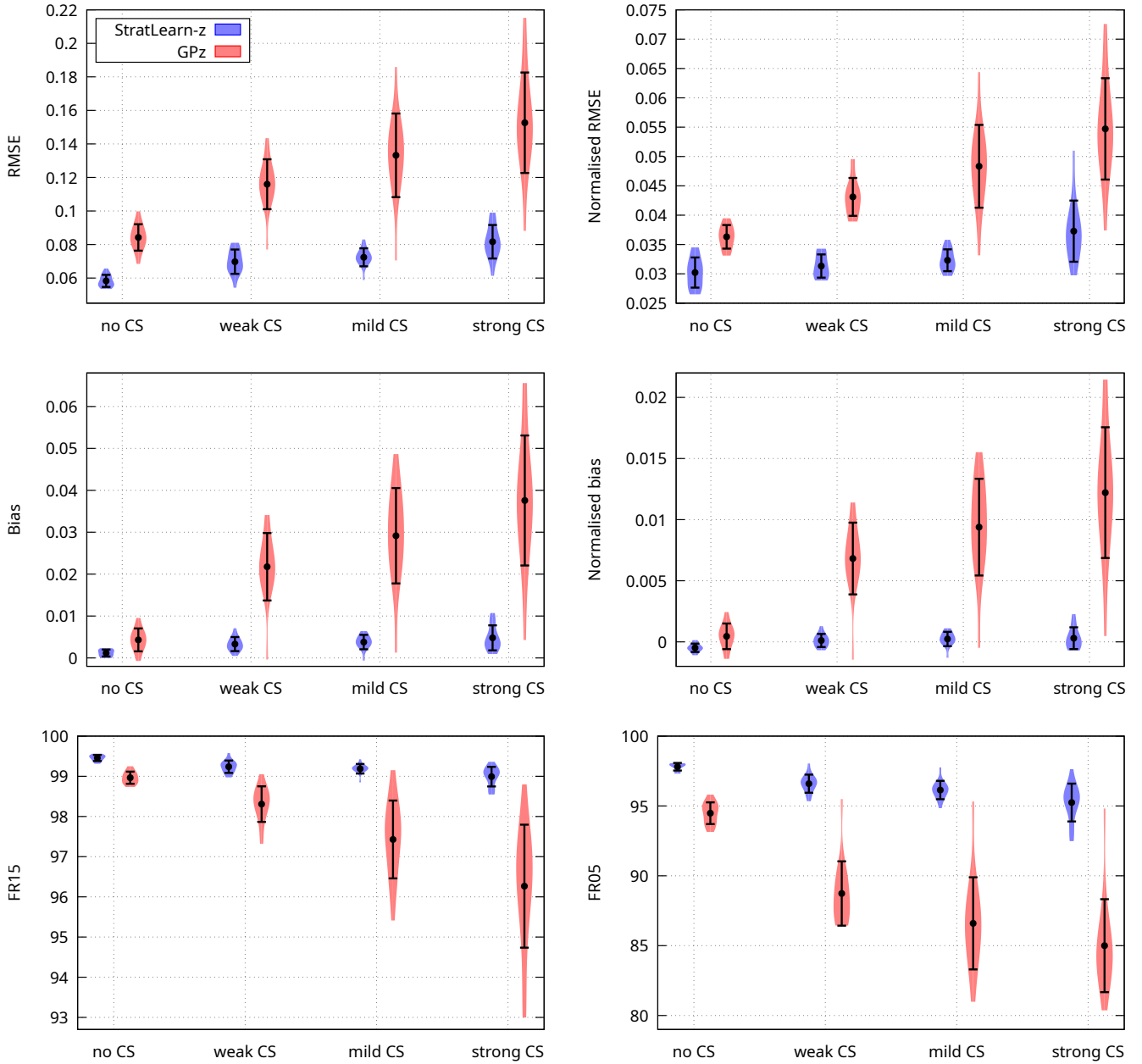


FIG. 8.— Violin plots showing the distribution of the metrics (averaged over 15 data realisations) for the four covariate shift scenarios. *StratLearn-z* results are shown in blue, while GPz results are shown in red. Black points with errorbars represent the mean and standard deviation for each case. There is a clear trend in the GPz results, which are strongly degraded by increasing covariate shift. On the other hand, the *StratLearn-z* results are only marginally impacted.

mulation of mass near 0.5 in the PIT distribution obtained from *StratLearn-z*, indicating an over-estimation of uncertainty in the conditional density estimates. However, the peak is centered at 0.5 and the distributions are symmetric, which suggests that most of the *StratLearn-z* conditional density estimates are well-centered around the true redshift values. Similar considerations hold for all covariate shift cases, highlighting once again the robustness of *StratLearn-z* results in presence of unrepresentative source datasets. On the other hand, the PIT distributions obtained from GPz are significantly flatter, but progressively less symmetric the stronger the covariate shift. We argue that the bump in the PIT distribution of *StratLearn-z*, although not ideal, is merely a symptom of our conditional

redshift distribution estimates being too broad, i.e., too conservative (see also Appendix C for a toy model demonstration). Additionally, we notice that the peaks at 0 and 1 in the PIT distributions are substantially lower for *StratLearn-z* compared to GPz, signaling a smaller fraction of catastrophic outliers for *StratLearn-z*, and they are below 1, which is the value they should take if PITs were evaluated with the perfectly specified conditional distributions.

5. CONCLUSIONS

We assess the performance of *StratLearn-z*, an implementation of the *StratLearn* method proposed in Autenrieth et al. (2024b) aimed at photo- z estimation. The method relies on

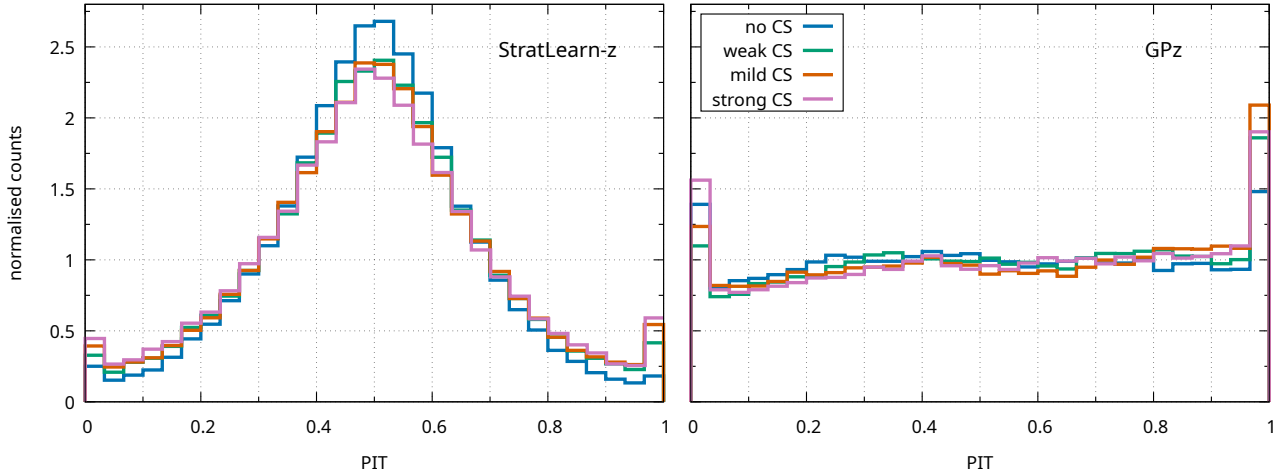


FIG. 9.— PIT distribution for *StratLearn-z* (left) and GPz (right) for all cases, as detailed in the legend: in blue the no CS case, in green the weak CS case, in orange the mild CS case and in green the strong CS case.

stratification of the source and target datasets based on estimated propensity scores, and is designed to improve the performance of ML algorithms for non-representative training datasets, i.e., in presence of covariate shift. We apply *StratLearn-z* to a simulated dataset of 100,000 galaxies (DeRose et al. 2019), where we enforce the presence of covariate shift by performing rejection sampling on the r -band magnitudes, following a similar approach as that of Freeman et al. (2017): this prescription is designed to approximately mimic observational bias in spectroscopic (source) datasets, which are biased towards brighter objects with respect to photometric (target) dataset. We vary the parameters involved in the rejection sampling procedure, thus obtaining four different source-target scenarios, with increasing levels of covariate shift. We then estimate propensity scores using logistic regression, and fit two full conditional density estimators to the resulting five strata, combining them via a weighted average. With our trained models we finally obtain predictions for the conditional redshift distributions of objects in the target datasets, which includes brighter and higher redshift objects with respect to the source set.

To evaluate the performance of *StratLearn-z*, we compute a number of metrics on the target predictions, and benchmark against results obtained from the GPz code (Almosallam et al. 2016a,b), using the version released with Stylianou et al. (2022). To obtain more robust estimates for the metrics and investigate their scatter, we randomly permute the full dataset and perform rejection sampling and model training 15 times, thus obtaining 15 sets of photo- z predictions (for each covariate shift scenario) from which we compute averaged metrics. We find *StratLearn-z* outperforms GPz for all metrics considered and for all degrees of covariate shift. Additionally, the *StratLearn-z* results are only marginally impacted by the unrepresentative training data, while GPz results are significantly degraded.

To evaluate the quality of the predicted conditional redshift distribution we plot the histogram of the PIT, for each covariate shift scenario and for both codes. While *StratLearn-z* seems to be overestimating the spread of the conditional redshift distribution, the PIT distribution shows a reduced fraction of catastrophic outliers and symmetry, with a large bump around 0.5, i.e., the *StratLearn-z* conditional densities appear well-centered around the true redshift values. Despite the overesti-

mation of photo- z pdf spread, we note that the PIT distribution for *StratLearn-z* is also consistent across covariate shift scenarios, highlighting again the robustness of the method. One assumption made in the paper is that the covariate shift assumption holds, i.e., there are no unmeasured (confounding) covariates that are predictive for redshift, and also associated to the selection process into source/target set. Covariate shift is often assumed when estimating photo- z , e.g. (Izbicki et al. 2017; Freeman et al. 2017), but may not be completely accurate for real data, e.g., when quality cuts are applied to the spectroscopic sample (Hartley et al. 2020), which in turn do not cover the same color-magnitude space as the photometric observation. Investigation of such violations will be the topic of a future work.

In summary, we found *StratLearn-z* provides stable predictions even in the most extreme scenario considered, in particular for high redshift regions where source/training data are lacking. Our analysis shows promising results, specifically concerning applications of the method to current and upcoming galaxy surveys, that will have to face the problem posed by incomplete and/or unrepresentative spectroscopic source sets to maximise the exploitation of photometric data.

Acknowledgements: CM’s work is supported by the Fondazione ICSC, Spoke 3 Astrophysics and Cosmos Observations, National Recovery and Resilience Plan (Piano Nazionale di Ripresa e Resilienza, PNRR) Project ID CN_00000013 “Italian Research Center on High-Performance Computing, Big Data and Quantum Computing” funded by MUR Missione 4 Componente 2 Investimento 1.4: Potenziamento strutture di ricerca e creazione di “campioni nazionali di R&S (M4C2-19)” - Next Generation EU (NGEU). RT acknowledges co-funding from Next Generation EU, in the context of the National Recovery and Resilience Plan, Investment PE1 – Project FAIR “Future Artificial Intelligence Research”. This resource was co-financed by the Next Generation EU [DM 1555 del 11.10.22]. RT is partially supported by the Fondazione ICSC, Spoke 3 “Astrophysics and Cosmos Observations”, Piano Nazionale di Ripresa e Resilienza Project ID CN00000013 “Italian Research Center on High-Performance Computing, Big Data and Quantum Computing” funded by MUR Missione 4 Componente 2 Investimento 1.4: Potenziamento strutture di ricerca e creazione di “campioni nazionali di R&S

(M4C2-19)’’ - Next Generation EU (NGEU). David van Dyk and Maximilian Autenrieth acknowledge partial support from the UK Engineering and Physical Sciences Research Council [EP/W015080/1, EP/W522673/1] and from the Marie-Skłodowska-Curie RISE [H2020-MSCA-RISE-2019-873089] Grant provided by the European Commission. RT and AM have been partially supported by the PRO3 Scuole Programme ‘DS4ASTRO’. This work used the *Julia* language and in particular the *DataFrames.jl*, *CSV.jl*, *Statistics.jl*, *Distances*, *GLM.jl* packages, and the *Gnuplot.jl* package for *Julia* to generate the

plots.

DATA AVAILABILITY

The original dataset used in this paper can be found at https://github.com/jfcrenshaw/pzflow/blob/main/pzflow/example_files/galaxy-data.pkl. We publicly release the version of *StratLearn* used for this work with example datasets – one for each covariate shift case considered – at github.com/chiamoretti/StratLearn-z

REFERENCES

- Abbott T. M. C., et al., 2018, *ApJS*, 239, 18
 Aihara H., et al., 2018, *PASJ*, 70, S8
 Akeson R., et al., 2019, *arXiv e-prints*, p. [arXiv:1902.05569](https://arxiv.org/abs/1902.05569)
 Almosallam I. A., Lindsay S. N., Jarvis M. J., Roberts S. J., 2016a, *MNRAS*, 455, 2387
 Almosallam I. A., Jarvis M. J., Roberts S. J., 2016b, *MNRAS*, 462, 726
 Amara A., Réfrégier A., 2007, *MNRAS*, 381, 1018
 Arnouts S., Cristiani S., Moscardini L., Matarrese S., Lucchin F., Fontana A., Giallongo E., 1999, *MNRAS*, 310, 540
 Autenrieth M., Wright A. H., Trotta R., van Dyk D. A., Stenning D. C., Joachimi B., 2024a, *arXiv e-prints*, p. [arXiv:2401.04687](https://arxiv.org/abs/2401.04687)
 Autenrieth M., van Dyk D. A., Trotta R., Stenning D. C., 2024b, *Statistical Analysis and Data Mining: The ASA Data Science Journal*, 17, e11643
 Benítez N., 2000, *ApJ*, 536, 571
 Bolzonella M., Miralles J. M., Pelló R., 2000, *A&A*, 363, 476
 Bordoloi R., Lilly S. J., Amara A., 2010, *MNRAS*, 406, 881
 Brammer G. B., van Dokkum P. G., Coppi P., 2008, *ApJ*, 686, 1503
 Brescia M., Cavauoti S., Razim O., Amaro V., Riccio G., Longo G., 2021, *Frontiers in Astronomy and Space Sciences*, 8, 70
 Carliles S., Budavári T., Heinis S., Priebe C., Szalay A. S., 2010, *ApJ*, 712, 511
 Carrasco Kind M., Brunner R. J., 2013, *MNRAS*, 432, 1483
 Carrasco Kind M., Brunner R. J., 2014, *MNRAS*, 438, 3409
 Cochran W. G., 1968, *Biometrics*, pp 295–313
 Collister A. A., Lahav O., 2004, *PASP*, 116, 345
 Crenshaw J. F., Kalmbach J. B., Gagliano A., Yan Z., Connolly A. J., Malz A. I., Schmidt S. J., The LSST Dark Energy Science Collaboration 2024, *AJ*, 168, 80
 D’Isanto A., Polsterer K. L., 2018, *A&A*, 609, A111
 Dawid A. P., 1984, *Journal of the Royal Statistical Society: Series A (General)*, 147, 278
 DeRose J., et al., 2019, *arXiv e-prints*, p. [arXiv:1901.02401](https://arxiv.org/abs/1901.02401)
 Euclid Collaboration et al., 2020, *A&A*, 644, A31
 Euclid Collaboration et al., 2024, *arXiv e-prints*, p. [arXiv:2405.13491](https://arxiv.org/abs/2405.13491)
 Firth A. E., Lahav O., Somerville R. S., 2003, *MNRAS*, 339, 1195
 Freeman P. E., Izbicki R., Lee A. B., 2017, *MNRAS*, 468, 4556
 Graff P., Feroz F., Hobson M. P., Lasenby A., 2014, *MNRAS*, 441, 1741
 Graham M. L., Connolly A. J., Ivezić Ž., Schmidt S. J., Jones R. L., Juric M., Daniel S. F., Yoachim P., 2018, *AJ*, 155, 1
 Hartley W. G., et al., 2020, *MNRAS*, 496, 4769
 Henghes B., Thyagalingam J., Pettitt C., Hey T., Lahav O., 2022, *MNRAS*, 512, 1696
 Heymans C., et al., 2021, *A&A*, 646, A140
 Hildebrandt H., et al., 2010, *A&A*, 523, A31
 Hildebrandt H., et al., 2021, *A&A*, 647, A124
 Ilbert O., et al., 2006, *A&A*, 457, 841
 Ivezić Ž., et al., 2019, *ApJ*, 873, 111
 Izbicki R., Lee A. B., Freeman P. E., 2016, *arXiv e-prints*, p. [arXiv:1604.01339](https://arxiv.org/abs/1604.01339)
 Izbicki R., Lee A. B., Freeman P. E., et al., 2017, *The Annals of Applied Statistics*, 11, 698
 Laureijs R., et al., 2011, *arXiv e-prints*, p. [arXiv:1110.3193](https://arxiv.org/abs/1110.3193)
 Ma Z., Hu W., Huterer D., 2006, *ApJ*, 636, 21
 Malmquist K. G., 1922, *Meddelanden fran Lunds Astronomiska Observatorium Serie I*, 100, 1
 Malmquist K. G., 1925, *Meddelanden fran Lunds Astronomiska Observatorium Serie I*, 106, 1
 Masters D., et al., 2015, *ApJ*, 813, 53
 Moreno-Torres J. G., Raeder T., Alaiz-Rodríguez R., Chawla N. V., Herrera F., 2012, *Pattern Recognition*, 45, 521
 Moskowitz I., Gawiser E., Crenshaw J. F., Andrews B. H., Schmidt S., The LSST Dark Energy Science Collaboration 2024, *arXiv e-prints*, p. [arXiv:2402.15551](https://arxiv.org/abs/2402.15551)
 Myles J., et al., 2021, *MNRAS*, 505, 4249
 Newman J. A., Gruen D., 2022, *ARA&A*, 60, 363
 Pasquet J., Bertin E., Treyer M., Arnouts S., Fouchez D., 2019, *A&A*, 621, A26
 Polsterer K. L., D’Isanto A., Gieseke F., 2016, *arXiv e-prints*, p. [arXiv:1608.08016](https://arxiv.org/abs/1608.08016)
 Porredon A., et al., 2022, *Phys. Rev. D*, 106, 103530
 Rau M. M., et al., 2023, *MNRAS*, 524, 5109
 Rosenbaum P. R., Rubin D. B., 1983, *Biometrika*, 70, 41
 Sadeh I., Abdalla F. B., Lahav O., 2016, *PASP*, 128, 104502
 Salvato M., Ilbert O., Hoyle B., 2019, *Nature Astronomy*, 3, 212
 Sánchez C., et al., 2014, *MNRAS*, 445, 1482
 Schmidt S. J., et al., 2020, *MNRAS*, 499, 1587
 Stylianou N., Malz A. I., Hatfield P., Crenshaw J. F., Gschwend J., 2022, *PASP*, 134, 044501
 Sugiyama S., et al., 2023, *Phys. Rev. D*, 108, 123521
 Tanaka M., et al., 2018, *PASJ*, 70, S9
 The LSST Dark Energy Science Collaboration et al., 2018, *arXiv e-prints*, p. [arXiv:1809.01669](https://arxiv.org/abs/1809.01669)
 Toribio San Cipriano L., et al., 2023, *arXiv e-prints*, p. [arXiv:2312.09721](https://arxiv.org/abs/2312.09721)
 Tosone F., Cagliari M. S., Guzzo L., Granett B. R., Crespi A., 2023, *A&A*, 672, A150
 Tutusaus I., et al., 2020, *A&A*, 643, A70

stratum for the redshift distributions. We focus on the worst case scenario, i.e., the strong CS case. Each panel of Fig. 15 refers to one of the five strata, except for the bottom right panel which shows the redshift distributions for the full source and target sets. Blue histograms refer to the source set, while orange histograms refer to the target set.

APPENDIX

A. DISTRIBUTIONS FOR ALL PHOTOMETRIC BANDS

As mentioned in Sec. 3.1, the introduction of covariate shift by rejection sampling on the *r*-band induces a shift also in the redshift distributions for source and target. Naturally, the effect is not limited to redshift, but also extends to other photometric bands. We plot here the distributions for all photometric bands (except for the *r*-band, already shown in Fig. 1), specifically Fig. 10 for the *u*-band, Fig. 11 for the *g*-band, Fig. 12 for the *i*-band, Fig. 13 for the *z*-band and Fig. 14 for the *y*-band. As in the main text, orange histograms represent the source dataset, while we show in blue the target dataset.

B. STRATIFICATION RESULTS

We show here the effectiveness of the stratification based on propensity scores in removing covariate shift within each

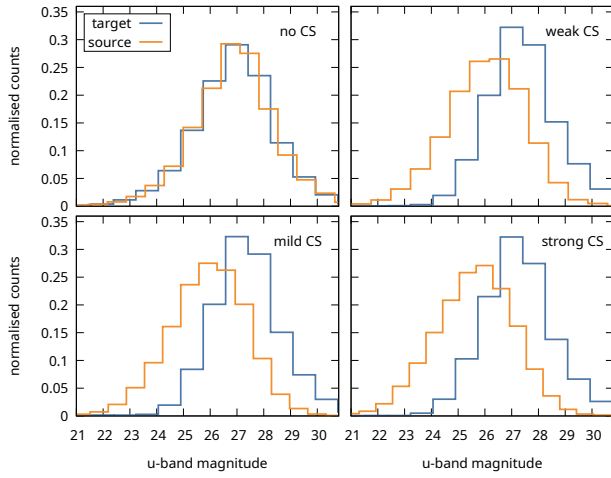


FIG. 10.— Source and target normalized distributions of u -band magnitudes for the four covariate shift cases, as stated in each panel. Orange histograms represent the source dataset, while in blue we plot the target datasets.

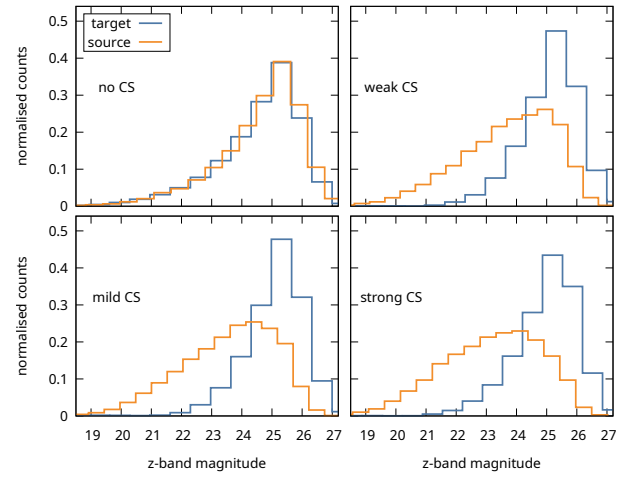


FIG. 13.— Same as Fig. 10 but for the z -band magnitudes.

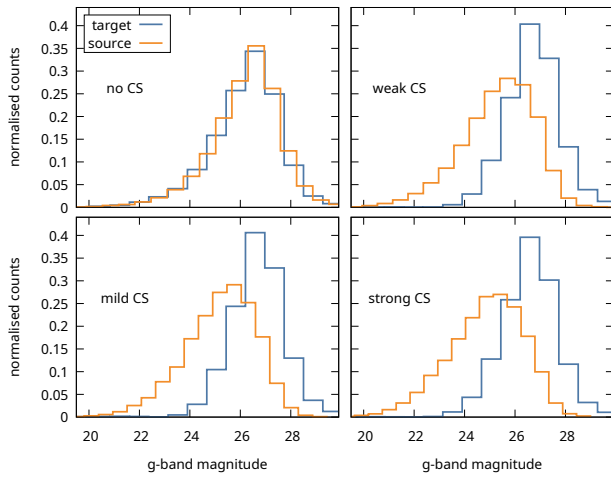


FIG. 11.— Same as Fig. 10 but for the g -band magnitudes.

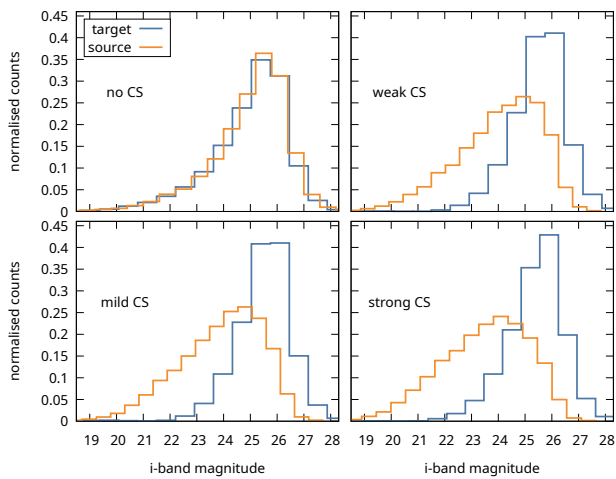


FIG. 12.— Same as Fig. 10 but for the i -band magnitudes.

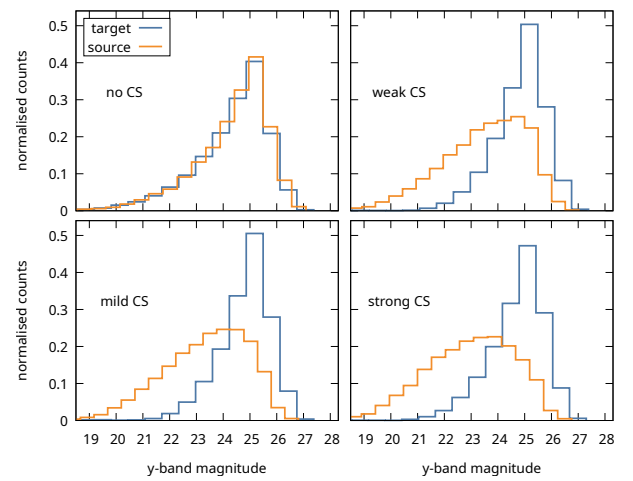


FIG. 14.— Same as Fig. 10 but for the y -band magnitudes.

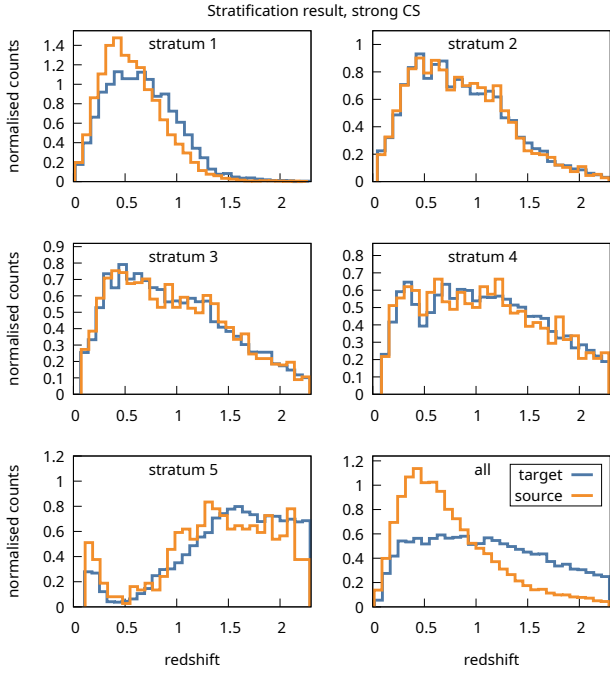


FIG. 15.— Same as Fig. 3 but for the redshift distributions. We note that this diagnostic is not possible in practice with real source/target data, as z is not observed in the target dataset.

C. TOY MODEL FOR PIT

In this section, we illustrate a simple toy example to demonstrate the effect on the PIT histograms when overestimating (or underestimating) the uncertainties/errorbars of (conditional) density estimates.

More precisely, we simulate data from $X_i \stackrel{\text{i.i.d.}}{\sim} N(\mu = 0, \sigma = 1)$, with $i = 1, \dots, n$, obtaining $n = 10,000$ independent samples. In a first step, we calculate the PIT assuming the correct model, i.e., $\text{PIT}_i = F_{X_i}(X_i)$, where $F_{X_i}(X_i)$ is the CDF of X_i evaluated at X_i . As expected, the resulting histogram exhibits a standard uniform distribution, as illustrated in Fig. 16 (left panel).

In a next step, we keep the same data simulating process, however, we assume a model with much larger uncertainties (centered at the correct location). More precisely, we calculate the PITs assuming a much broader Gaussian distribution, i.e., we calculate $\text{PIT}_i = F_{X'_i}(X_i)$, where $F_{X'_i}(X_i)$ is the CDF of a random variable $X'_i \sim N(\mu = 0, \sigma = 2)$, evaluated at X_i . Plotting the histogram of PIT values in Fig. 16 (center panel), we find a large (symmetric) bump around 0.5, with less mass towards the edges zero and one.

Third, we assume a model that underestimates the uncertainties, i.e., we calculate the PITs via $\text{PIT}_i = F_{X''_i}(X_i)$, where $F_{X''_i}(X_i)$ is the CDF of a random variable $X''_i \sim N(\mu = 0, \sigma = 0.8)$, evaluated at X_i . As illustrated in right panel of Fig. 16, this leads to large peaks at the edges (zero and one), indicating a large number of true values (from X_i) laying outside the

assumed model distributions. (We note that similar peaks at the edges can be obtained by systematically shifting the center of the assumed model distribution away from the center of the underlying data-generating distributions).

We note that center panel of Fig. 16 exhibits a similar pattern as the PIT histograms obtained for the *StratLearn-z* conditional density estimates in Fig. 9. The symmetric bump in the PIT histogram around 0.5 indicates that a large proportion of the conditional density estimates are well centered around the true values (as also suggested by the low RMSE and low mean error of *StratLearn-z*, as presented in Table 2). However, there is an overestimation of uncertainties/errorbars in the conditional density estimates (overly conservative estimates). On the contrary, underestimating uncertainties leads to large peaks of the PIT histograms at the edges (zero and one) indicating larger fractions of (catastrophic) outliers as it has been observed for the GPz estimates. Finally, while in the optimal case the PIT histograms exhibit a flat uniform distribution (as illustrated in left panel of Fig. 16), we argue that an overly conservative estimate of the uncertainties (with estimates well-centered around the true values) is more desirable than underestimating the uncertainties, which might lead to catastrophic outliers and a disproportionate number of estimates which do not cover the true values.

This paper was built using the Open Journal of Astrophysics L^AT_EX template. The OJA is a journal which provides fast and easy peer review for new papers in the `astro-ph` section of the arXiv, making the reviewing process simpler for authors and referees alike. Learn more at <http://astro.theoj.org>.

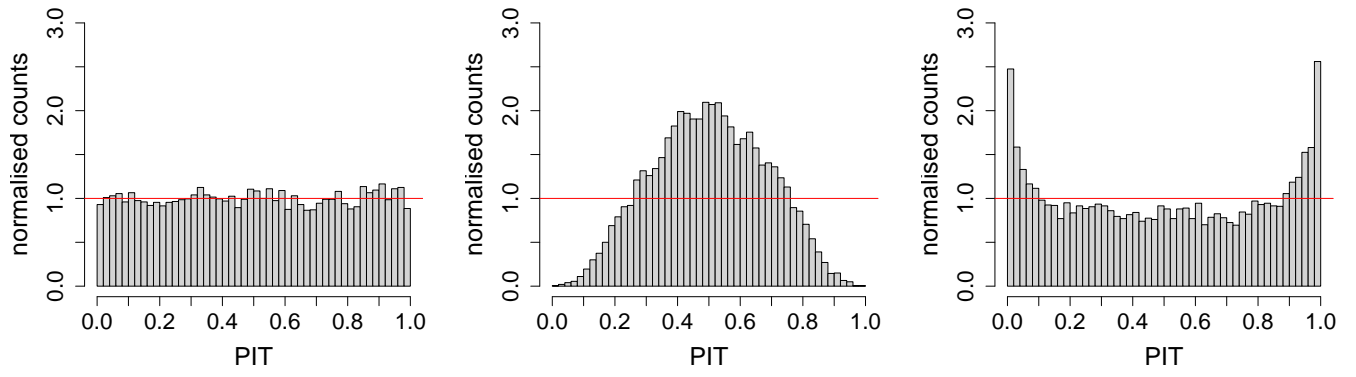


FIG. 16.— PIT distributions illustrating the toy examples introduced in Appendix C. Left panel: correct model; center panel: overestimated uncertainties; right panel: underestimated uncertainties.